

NEAR-INFRARED CORONAL LINES IN NARROW-LINE SEYFERT 1 GALAXIES

A. RODRÍGUEZ-ARDILA^{1,2} AND S. M. VIEGAS

Instituto de Astronomia, Geofísica e Ciências Atmosféricas – Universidade de São Paulo, Rua do Matão 1226, CEP 05508-900, São Paulo, SP, Brazil

M. G. PASTORIZA

Departamento de Astronomia - UFRGS. Av. Bento Gonçalves 9500, CEP 91501-970, Porto Alegre, RS, Brazil

AND

L. PRATO¹

Department of Physics and Astronomy, UCLA, Los Angeles, CA 90095-1562

Accepted to the Astrophysical Journal

ABSTRACT

We report spectroscopic observations in the wavelength region $0.8\mu\text{m} - 2.4\mu\text{m}$ aimed at detecting near-infrared coronal lines in a sample of 5 narrow-line and 1 broad-line Seyfert 1 galaxies. Our measurements show that $[\text{Si VI}] 1.963\mu\text{m}$, $[\text{S IX}] 1.252\mu\text{m}$ and $[\text{S VIII}] 0.991\mu\text{m}$ are present in most of the objects and are useful tracers of nuclear activity. Line ratios between coronal and low-ionization forbidden lines are larger in narrow-line Seyfert 1 galaxies. A positive correlation between FWHM and ionization potential of the forbidden lines is observed. Some coronal lines have widths similar to that of lines emitted in the broad line region (BLR), indicating that part of their flux originates in gas close to the outer portions of the BLR. Most coronal lines are blueshifted relative to the systemic velocity of the galaxy and this shift increases with the increase in line width. Assymmetries towards the blue are observed in the profiles of high-ionization Fe lines, suggesting that the emitting gas is related to winds or outflows, most probably originating in material that is being evaporated from the torus. This scenario is supported by models that combine the effects of shock ionization and photoionization by a central continuum source in the gas clouds. The agreement between the coronal line emission predicted by the models and the observations is satisfactory; the models reproduced the whole range of coronal line intensities observed. We also report the detection of $[\text{Fe XIII}] 1.074, 1.079\mu\text{m}$ in three of our objects and the first detection of $[\text{P II}] 1.188\mu\text{m}$ and $[\text{Ni II}] 1.191\mu\text{m}$ in a Seyfert 1 galaxy, ARK 564. Using the ratio $[\text{P II}]/[\text{Fe II}]$ we deduced that most Fe present in the outer NLR of ARK 564 is locked up in grains, and the influence of shocks is negligible.

Subject headings: galaxies: Seyfert – radiation mechanisms — galaxies: nuclei

1. INTRODUCTION

Coronal lines are collisionally excited forbidden transitions within low-lying levels of highly ionized species ($\chi \geq 100$ eV). They can be formed either in gas photoionized by a hard UV continuum (Grandi 1978; Korista & Ferland 1989; Ferguson, Korista & Ferland 1997) or in a very hot, collisionally ionized plasma (Viegas-Aldrovandi & Contini 1989). It is also possible that the excitation mechanism is a mixture of collisional ionization at the shock front and photoionization in the emitting clouds (Contini & Viegas 1992; Viegas & Contini 1994; Contini, Prieto & Viegas 1998). In active galactic nuclei (AGN), the presence of coronal lines, mainly in the optical region (i.e. $[\text{Fe VII}]$ and $[\text{Fe X}]$), have long been known to be common features in the spectra of these sources, although the physical conditions of the gas from which they originate and the location of the emitting region are still poorly determined.

Observationally, coronal lines are, on average, broader and blueshifted, relative to the centroid position, of lines of lower ionization stages such as $[\text{O III}]\lambda 5007$ (De Roberties & Osterbrock 1984, 1986; Veilleux 1991; Erkens, Appenzeller & Wagner 1997). This has led to the speculation that they are formed in a separate region, known as the coronal line region (CLR), located at an intermediate distance between the classi-

cal narrow line region (NLR) and the broad-line region (BLR). Variability studies on $[\text{Fe VII}] \lambda 6087$ and $[\text{Fe X}] \lambda 6374$ carried out by Veilleux (1988) also suggest that the most likely place for the CLR is between the BLR and NLR. Erkens, Appenzeller & Wagner (1997) found that the coronal line emission occurs predominantly in objects with a soft X-ray excess and suggested a relationship between these lines and the X-ray absorption edges (also known as warm absorbers) seen in 50% of AGN. In fact, Porquet et al. (1999) demonstrated through photoionization modeling that the optical coronal lines could be formed in the warm absorber and that they may strongly constrain the physical parameters of that medium. However, the number of coronal lines effectively detected in the optical region is small ($[\text{Fe VII}] \lambda 5721, \lambda 6087$; $[\text{Fe X}] \lambda 6374$; $[\text{Fe XI}] \lambda 7892$ and $[\text{Fe XIV}] \lambda 5303$). It is then necessary to expand the range of important diagnostics of the physical conditions that prevail in the coronal gas to other wavelength intervals. In this respect, the near-infrared (NIR) is promising because it offers a wealth of highly ionized species different from Fe.

Until now, coronal line emission between $1.5\mu\text{m}$ and $4\mu\text{m}$ has been detected in only a small number of AGN. Oliva & Morwood (1990) reported, for the first time, the observation of $[\text{Si VI}] 1.962\mu\text{m}$ and $[\text{Si VII}] 2.483\mu\text{m}$ in the archetypical Seyfert 2 galaxy NGC 1068. Oliva et al. (1994) detected, in ad-

¹ Visiting Astronomer at the Infrared Telescope facility, which is operated by the University of Hawaii under contract from the National Aeronautics and Space Administration

² e-mail address: ardila@astro.iag.usp.br

dition to those two lines, [S IX] $1.252\mu\text{m}$, [Ca VIII] $2.321\mu\text{m}$ and [Si IX] $3.9346\mu\text{m}$ in Circinus, another nearby Seyfert 2 nucleus. Marconi et al. (1994) detected [Si VI] $1.962\mu\text{m}$ in eight AGN (including the former two objects) in a sample composed of Seyferts, Starburst and Ultraluminous Infrared Galaxies (ULIRGs). They concluded that [Si VI] emission was a common characteristics of Seyfert nuclei, consistent with modeling the line formation by photoionization of the active nucleus. That result had reinforced the use of [Si VI] $1.962\mu\text{m}$ as a diagnostic of AGN activity and had allowed the detection of hidden AGN, mostly in ULIRGs samples (Veilleux, Sanders & Kim 1999; Murphy et al. 2000). Thompson (1995) studied NGC 4151 in detail and reported the detection of several coronal lines in the $0.87\mu\text{m} - 2.5\mu\text{m}$ interval, most notably [S VIII] $0.911\mu\text{m}$, [Fe XIII] $1.074, 1.079\mu\text{m}$, [S IX] $1.252\mu\text{m}$, [Si VI] $1.963\mu\text{m}$ and [Si VII] $2.481\mu\text{m}$. Gianuzzo, Rieke & Rieke (1995) studied a sample of six Seyfert 1 galaxies (one of them NGC 4151) in the $2\mu\text{m}$ region and detected [Si VI] $1.963\mu\text{m}$ in all the galaxies and [Ca VIII] $2.321\mu\text{m}$ in two of them.

In this paper we present the results of a search for coronal emission lines in the wavelength range $0.8\mu\text{m} - 2.5\mu\text{m}$ by means of long-slit spectroscopy at moderate resolution ($R \sim 750$). The sample chosen for this study is composed of six Seyfert 1 galaxies, five of them classified as narrow-line Seyfert 1 (NLS1). These data are the first measurements of coronal lines in the NIR made on this sub-class of objects. Here, we concentrate on the analysis of the line ratios derived from our measurements and the physical conditions for the CLR that they imply. We also discuss the kinematics of the CLR based on the analysis of the line profiles. In addition, we report the detection of other forbidden lines and molecular lines emitted by the NLR in the NIR, which are also useful for constraining the various excitation models proposed so far.

Our observations are described in § 2, the main results in § 3, the study of the kinematics of the CLR in § 4 and the physical conditions for the CLR derived from the observations in § 5. Some comments about the low ionization and coronal lines observed appear in § 6. We present the main conclusions of this work in § 7.

2. OBSERVATIONS AND DATA REDUCTION

NIR spectra providing continuous coverage between $0.8\mu\text{m}$ and $2.4\mu\text{m}$ were obtained at the NASA 3 m Infrared Telescope Facility (IRTF) on 2000 October 11 (UT) with the SpeX facility spectrometer (Rayner et al. 1998). The detector consists of a 1024×1024 ALADDIN 3 InSb array with a spatial scale of $0.15''/\text{pixel}$. Simultaneous wavelength coverage was obtained by means of prism cross-dispersers. A $0.8'' \times 15''$ slit was used during the observations, giving a spectral resolution of 320 km/s . The seeing was near $1''$ during the exposures.

Details of the spectral extraction and wavelength calibration procedures are given in Rodríguez-Ardila et al. (2002a). The spectral resolution provided by SpeX was sufficiently high so that except for a few particular cases, the lines emitted by the NLR were spectroscopically resolved.

Table 1 lists the objects observed and their main characteristics. There are several reasons for the predominance of NLS1 in the sample. These objects usually show stronger and more luminous optical coronal lines than other AGNs (Rodríguez-Ardila, Pastoriza & Donzelli 2000). In the X-ray, NLS1s outnumber other AGN in regard to the presence of soft X-ray ex-

cesses, allowing to study the link between X-rays and coronal line intensity. NLS1 emission lines, even those formed in the BLR, are sufficiently narrow to allow an easier deblending of adjacent emission features. These characteristics make NLS1s optimal targets for studying coronal lines and their relationship with the NLR and BLR.

The calibrated spectra were corrected for Galactic extinction, as determined from the *COBE/IRAS* infrared maps of Schlegel, Finkbeiner & Davis (1998). The value of the Galactic $E(B-V)$ is listed in Table 1. Finally, each spectrum was shifted to rest wavelength. The value of z adopted was determined by averaging the redshift measured from the strongest lines, usually O I $\lambda 8446$, [S III] $\lambda 9531$, Fe II $\lambda 9997$, Pa δ , He I $\lambda 10830$, O I $\lambda 11287$, Pa β , Pa α and Br γ . In all cases, the radial velocities were in very good agreement with the values reported in the literature.

In addition to the NIR data, optical spectra for 1H 1934-063, MRK 335, TON S 180 and MRK 1044 were available in the wavelength region that includes the [Fe VII] $\lambda 5721$ and [Fe X] $\lambda 6374$ lines. There is also data covering the [Fe XI] $\lambda 7894$ line for 1H 1934-063. Details of these observations and the reduction procedure are described elsewhere (Rodríguez-Ardila, Pastoriza & Donzelli 2000; Rodríguez-Ardila et al. 2002b). Before making any measurements using the optical spectra, they were also corrected for Galactic extinction (see values in Table 1). These data will be used along with the NIR spectra to study the kinematics and physical conditions of the CLR.

3. RESULTS

Figures to show the most important NIR narrow lines, including the coronal lines, observed in the galaxies. The measured line fluxes are summarized in Table 2. The errors quoted reflect solely the 2σ uncertainty in the placement of the continuum and in the S/N around the line of interest. Fluxes were measured by fitting Gaussians to each emission feature and the continuum underlying each line was approximated by a low-order polynomium. In all cases, the NLR lines were well described by a single Gaussian component. Measurements of [Si VI] $1.963\mu\text{m}$ and [Ca VIII] $2.321\mu\text{m}$ were complicated by poor atmospheric transmission near the former and the presence of deep CO $\Delta\nu = 2$ bands in the latter. However, the residuals around the features of interest, after dividing the target spectra by that of the telluric star, are low enough in most objects to allow an unambiguous identification of the lines.

In addition to the coronal lines, Table 2 also list the fluxes of other forbidden and permitted lines detected in the NIR spectra. We found that [S III] $0.953\mu\text{m}$ is, by far, the strongest of all narrow forbidden lines and one of the brightest lines in the NIR range, particularly in 1H 1934-063 and ARK 564. Molecular H₂ emission is also observed in these two objects as well as in the broad-line Seyfert 1 galaxy NGC 863.

[Fe XIII] $1.074\mu\text{m}$ is observed unambiguously in 1H 1934-063 (Fig.), ARK 564 (Fig.), MRK 335 (Fig.) and TON S 180. That line has only been reported before in NGC 4151 (Thompson 1995) and NGC 1068 (Oliva et al. 2001). Evidence of the companion [Fe XIII] $1.079\mu\text{m}$ line is seen in 1H 1934-063 and ARK 564 but it is too blended with He I $1.083\mu\text{m}$ to allow a confident measurement of its flux. [P II] $1.188\mu\text{m}$ and [Ni II] $1.191\mu\text{m}$ are observed in ARK 564 (see Figure). The only previous identification of [P II] in an extragalactic object was in NGC 1068 (Oliva et al. 2001). [Ni II], to our knowledge, was never reported in an extragalactic source. Its presence indicates

gas with densities below 500 cm^{-3} , which is the critical density of that line.

Our data show that not all AGN display coronal lines. In fact, except for a few lines, they are not detected above the noise level in MRK 1044 and TONS 180. In this latter object, the only coronal line detected was [Fe XIII]. In contrast, 1H 1934-063 and Ark 564 display very rich CLR spectra, with bright [Si VI] $1.963 \mu\text{m}$, [Si X] $1.430 \mu\text{m}$, [S IX] $1.252 \mu\text{m}$, [S VIII] $0.991 \mu\text{m}$ and detectable [Ca VIII] $2.321 \mu\text{m}$. MRK 335 seems to be an intermediate case, with detectable emission at the expected position of most lines.

The above findings agree with those of Marconi et al. (1994), who conducted a survey of [Si VI] $1.962 \mu\text{m}$ in 26 galaxies, 15 of them classified as Seyferts. They detected this line in some but not all of the AGN in their sample. They interpreted their results as indicating that either the conditions required to produce bright coronal lines are not always met or the $2 \mu\text{m}$ extinction toward the CLR is too large in the objects in which it was not observed.

It is important to compare the similarity of the NLR spectra of the different objects of our sample in the NIR region. For this purpose, line ratios between coronal and forbidden low-ionization lines were calculated, as is shown in Table 3. Compared to data published in the literature for the Seyfert 2 galaxies NGC 1068 and Circinus and the broad-line Seyfert 1 NGC 4151, some line ratios in the NLS1 exhibit different behavior. [S IX] $1.252 \mu\text{m}$ /[Fe II] $1.257 \mu\text{m}$, for instance, is six times stronger in ARK 564 than in Circinus and 12 times larger than in NGC 4151. [S VIII] $0.991 \mu\text{m}$ /[Ca I] $0.985 \mu\text{m}$ is larger in ARK 564 than in Circinus and NGC 1068, by factors of 5 and 12 respectively. This trend is also observed in line ratios involving coronal and molecular lines, for example as in [Ca VIII] $2.321 \mu\text{m}$ /H₂ $2.121 \mu\text{m}$. This ratio is up to four times higher in 1H 1934-063 than in Circinus. Although it is not possible to draw any definitive conclusions on this matter because of the small number of objects, there is the tendency for NLS1 to display extreme values of a given ratio, even compared to broad-line Seyfert 1 objects. Whatever the case, it cannot be the result of reddening because every line pair involved in the ratios listed in Table 3 are so close in wavelength that they are free from this effect.

Table 4 lists the line fluxes of the coronal lines measured from the optical spectra. For ARK 564 the data were taken directly from Erkens, Appenzeller & Wagner (1997). Although the slit width used in the optical spectroscopy was larger than in the NIR ($2''$ and $0.8''$, respectively), it has little effect on the high excitation lines when combining data from these two spectral regions. A careful inspection of the 2-D frames at the expected position of the coronal lines does not reveal any sign of extended emission. Spatially, the CLR emission is indistinguishable from the unresolved nuclear emission. Similar results are reported for NGC 1068 (Marconi et al. 1996) and Circinus (Oliva et al. 1994). Nonetheless, we recall that the galaxies in our sample are located at relatively large distances ($42 \leq D \leq 148 \text{ Mpc}$), meaning that an upper limit to the size of the CLR based on the FWHM of the unresolved nucleus (in the $0.8''$ resolution case) would vary from 150 pc in 1H 1934-063 to 950 pc in TONS 180. For the latter object, that size is large enough to include the extended narrow line region, but only one coronal line was detected. For the former, the CLR is well within the NLR limits. Additional constraints on the location of the CLR can be obtained by the study of the line profiles and the

kinematics they imply.

4. KINEMATICS OF THE CLR

The presence of correlations between the widths of forbidden optical lines and the ionization potential (IP) and critical density (N_{crit}) of the corresponding transition have been reported in several samples of Seyfert galaxies (De Roberties & Osterbrock 1984, 1986; Evans 1988). This result was interpreted in terms of a stratified NLR in which high ionization lines (i.e. coronal lines) are emitted in the inner NLR or even in the transition region between the NLR and BLR. Lower ionization lines (i.e. [O I], [S II], and [N II]) originate in the outer portions of the NLR.

Nonetheless, according to the published literature, when NIR coronal lines are involved, the correlations are not as clear as those observed with optical lines. Giannuzzo, Rieke & Rieke (1995) studied a sample of six Seyfert 1 galaxies in the $2 \mu\text{m}$ region. They detected [Si VI] $1.96 \mu\text{m}$ in all the galaxies and found that its width varied from very narrow profiles ($\sim 300 \text{ km s}^{-1}$) to profiles approaching that of the broad lines ($\sim 2200 \text{ km s}^{-1}$). [Ca VIII] $2.32 \mu\text{m}$, detected in two objects of Giannuzzo et al.'s sample, showed no correlation with the [Si VI] width, even though they have IPs of the same order (127 eV and 167 eV, respectively). Knop et al. (1996), in their spatially resolved $1.24-1.30 \mu\text{m}$ spectroscopy of NGC 4151, found [S IX] $1.252 \mu\text{m}$ to be narrower than Pa β (narrow component) and almost 2.5 times narrower than the low-ionization line [Fe II] $1.2567 \mu\text{m}$, for which they measured a FWHM of 400 km s^{-1} . Combining Giannuzzo et al.'s data with that of Knop et al. (1996) for NGC 4151, no correlation between IP and coronal line width is observed.

Similar results have been reported when NIR lines of Seyfert 2 galaxies are studied. In NGC 1068 (Marconi et al. 1996) no trend between IP and FWHM is observed. Low and high ionization lines have similar FWHM ($\sim 1000 \text{ km s}^{-1}$). Oliva et al. (1994), in their study of the Circinus galaxy, reported that all the visible and IR coronal lines were quite narrow and only barely resolved, with intrinsic widths of less than 100 km s^{-1} .

Table 5 lists the FWHM, already corrected for instrumental width, and the shift of the line centroid with respect to the systemic velocity of the galaxy, for the forbidden lines reported in Table 2. MRK 1044 and TONS 180 were not included because they lack significant coronal line emission. Also listed in Table 5 are the FWHM and shifts measured for the optical coronal lines [Fe VII], [Fe X] and [Fe XI] measured in 1H 1934-063, ARK 564 and MRK 335.

4.1. Correlations between line width, ionization potential and critical density

Several interesting results arise from the data listed in Table 5. In 1H 1934-063, ARK 564 and MRK 335, there is a clear correlation between line width and IP, as can be graphically seen in Figure . No correlation is observed for NGC 863. This fact can be explained if we recall that most NLR lines in that object were unresolved and/or detected only as upper limits. Except for [S VIII] $0.991 \mu\text{m}$ (IP=280 eV), the lines of NGC 863 plotted in Figure have FWHM equal to the instrumental value. Overall, low-ionization lines (i.e. [Ca I], [Fe II]) are characterized by values of FWHM lower than those of the highest ionized species (i.e. [Fe XIII] and [Si X]). In 1H 1934-063, for example, there is up to a factor of four difference in FWHM between low and high ionization lines. Figure shows

the presence of a zone of avoidance in width for lines of small IP. No low ionization lines are found in the upper left corner of the plot, the region of large FWHM and small IP. Assuming that the width of the lines reflects the bulk motion of the emitting clouds in the gravitational potential of the central mass concentration, our results imply that low ionization lines are preferentially emitted in the outermost portion of the NLR. Among coronal lines, we notice a spread in line width, the most noticeable being the case of [S IX], which is as narrow as [Fe II]. However, this fact does not contradict our results, mainly because we found evidence that ions of different species follow a different slope for the FWHM-IP correlation.

In effect, the left panels of Figure show that for 1H 1934-063, ARK564 and MRK 335, the sources with the most conspicuous CLR spectrum, the width of the iron lines increases faster with the IP than that of sulfur and silicon. [Si X] 1.430 μ m, the line with the largest IP (351 eV), is not the broadest one. [Fe XIII] 1.074 μ m, with a slightly smaller IP (331 eV), is significantly broader than [Si X]. [S IX] 1.252 μ m (IP=328 eV), another high-ionization coronal line, has a width comparable to those of low-ionization lines (nonetheless, this line was not detected in MRK 335). In 1H 1934-063, there is a slight decrease in line width between [Fe X] and [Fe XI], not observed in ARK 564 and MRK 335. But clearly, when the degree of ionization of the iron lines increases, the trend is to increase the line width, also.

A similar tendency is observed when the gas kinematics are plotted against the critical density (N_{crit}) of the different transitions, as can be seen in the right panels of Figure . For 1H 1934-063, we observe that the gas emitting the sulfur lines has different kinematics than that emitting the iron or silicon lines, as previously suggested. As in the case of the ionization potential, the width of the sulfur lines is insensitive to the increase of the critical density. For ARK 564 and MRK 335, all lines of different species tend to positively correlate with N_{crit} , reinforcing the hypothesis of a stratified CLR. Nonetheless, it should be kept in mind that the critical densities of high ionization NIR lines are lower than those of the optical region, even though the degree of ionization of a particular ion increases. This fact may create an artificially weaker correlation between FWHM and N_{crit} compared to that observed between FWHM and IP.

4.2. Evidences for outflows in the CLR

Why do different species not follow a similar FWHM – IP or FWHM – N_{crit} correlation? Clues to the answer can be obtained by examining the values of ΔV exhibited by the coronal lines (see Table 5 and Figure). While low-ionization lines have no shifts at all or are redshifted by a small amount, coronal lines are characterized by large blueshifts, the largest ones being for the lines with the largest IP (≥ 300 eV) and FWHM. Both in 1H 1934-063 and ARK 564, the increase/decrease in blueshift clearly accompanies the increase/decrease in line width and IP for lines of the same species: [Fe XIII] is broader and more blueshifted than [Fe VII]. Interestingly, and most importantly, [Fe XIII], the broadest coronal line, is the most blueshifted line in these two objects. [Si X] and [S IX], with IP similar to that of the former, but significantly narrower, are less blueshifted. In 1H 1934-063, the decrease in line width when going from [Fe X] to [Fe XI] is also accompanied by a decrease in blueshift. MRK 335 behaves somewhat differently. While [Fe XIII] is again the broadest coronal line, the most blueshifted one is [Si X]. In addition, iron lines of different IP seem to be char-

acterized by a similar shift. It is also important to note that in this object the sulfur and silicon gases have rather similar kinematics but, as in the other two objects, different from that of iron. For the remaining three galaxies (NGC 863, MRK 1044 and TON S 180), nothing can be said about the kinematics of the CLR due to the lack of sufficient information. Nonetheless, it seems that when significant coronal line emission is detected, the iron lines manifest different kinematics than the rest of the coronal lines. Although at the present time it is not possible to establish how significant is the result found for Fe because of the small number of objects, we consider that the results are highly encouraging and lead towards a breakthrough in the current understanding of the CLR.

If the blueshift of the lines is interpreted as being attributable to an outflow of coronal gas towards the observer, what is the approximate location of such a flow? Figure is useful for addressing this question. There, we see that the FWHM of [Fe XIII] and [Si X] are larger than that of O I 1.128 μ m. Permitted O I emission is a feature completely associated with the BLR (Grandi 1980; Morris & Ward 1989). Very recently, Rodríguez-Ardila et al. (2002b) presented observational evidence that this line arises in the outer boundary of that region. Therefore, our data suggest that part of the CLR is located in the boundary between the BLR and NLR. At this location, a natural scenario for the origin of the flow is, for example, radiatively accelerated material evaporated from the outer regions of the accretion disk and/or inner walls of the torus, as suggested by Erkens, Appenzeller & Wagner (1997) for ARK 564 (and other objects). Pier & Voit (1995) had already proposed a similar scenario in which molecular clouds located at the inner edge of the torus are heated, ionized and evaporated by intense UV/X-ray radiation from the AGN. Another possibility is interaction between the radio jet and ambient gas. Nonetheless, the NLS1 of our sample are radio-quiet objects. In addition, studies in the optical region aimed at detecting coronal lines in radio-loud AGN (Appenzeller & Wagner 1991; Erkens, Appenzeller & Wagner 1997) have found that these objects lack significant coronal line emission, giving little support to this latter hypothesis.

4.3. Ionization structure of the CLR

Based on the results from the above section, we propose a CLR in which high ionization iron and silicon lines are formed in the borderline between the BLR and NLR, the bulk of the [Fe XIII] line being emitted closest to the torus. Farther out, but yet in the BLR–NLR interface, [Fe X], [Fe XI] and [Si X] are formed. The remaining forbidden lines would be emitted in the classical NLR. A good test for this scenario is the analysis of a sample composed of Seyfert 1 and 2 galaxies. It is expected that the latter objects show little or no [Fe XIII], as is already the case for NGC 1068 and Circinus. Also consistent with this scenario is the lack of correlation between the FWHM and IP and N_{crit} of high-ionization coronal lines in Seyfert 2s. The lines emitted closest the torus are partially hidden from direct view under certain orientation angles. For Seyfert 1s, if the conditions for forming coronal lines are met, they are observed in all their extent.

5. PHYSICAL PROPERTIES OF THE CLR

Based on the results of the above section, important clues about the physical conditions and excitation mechanisms of the coronal gas in Seyfert galaxies can be drawn. As Table 3 shows,

the NLR of the objects is characterized by a mixture of intense low and high ionization lines. While the latter lines are blueshifted relative to the systemic velocity of the host galaxy, the former are, in general, coincident with the rest position of the line.

The above means that at least two different components are needed in order to explain the observed NLR spectrum: one set of clouds producing low to intermediate ionization lines (i.e. [Ca I], [S III]) and another set, closer to central source, and responsible for coronal lines (i.e. [Si VI], [Fe X], [S VIII]). In this section, based on current photoionization models, we make rough estimates of the necessary conditions responsible for the emission of coronal lines. A detail modeling of the whole NLR spectrum for the individual objects (ARK 564, 1H 1934-063 and MRK 335) is left for a future paper.

Table 6 lists ratios between optical and NIR coronal lines, found in 1H 1934-063 and ARK 564. The values listed are corrected for internal reddening, derived from the Balmer decrement assuming an intrinsic ratio of 3.1. For the former galaxy, the E(B-V) was determined by Rodríguez-Ardila, Pastoriza & Donzelli (2000) while for the latter, it was taken from Erkens, Appenzeller & Wagner (1997). We have chosen these two objects because all coronal lines between $0.5\mu\text{m}$ and $2.5\mu\text{m}$ predicted by models are observed in these two sources. For comparison, data for NGC 1068 and Circinus (also reddening corrected) are included.

It is interesting to see that the four AGN have similar values of most line ratios, differing by less than a factor of 3. The exception is NGC 1068, which presents extreme values in the ratios [Fe X]/[Fe VII] and [S IX]/[Si VI]. This was already noted by Marconi et al. (1996) in their analysis of the NIR and visible coronal lines of that object. They found that NGC 1068 has a somewhat lower ionization CLR, which they attributed to either a steeper ionizing continuum or a somewhat lower ionization parameter.

Assuming that the coronal lines are formed by the combination of photoionizing radiation from the active center and a shock front (from the evidence discussed in the previous section), we have compared the observed coronal line ratios with the grid of model predictions of Contini & Viegas (2001). The simulations apply whether the shocks originate from a radial outflow of clouds (if evaporated material from the torus give rise to the coronal lines) or from an interaction of the emitting clouds with a radio jet.

Table 6 shows the predictions of the different models obtained by varying the shock velocity and the preshock densities, keeping constant the geometrical thickness of the clouds and the intensity of the photoionizing radiation of the central source. Also listed in Table 6 are the predictions of the best fitting model obtained for Circinus by Contini, Prieto & Viegas (1998). It was obtained from a suitable combination of clouds, taking into account the effect of geometrical dilution and a weighted average of single cloud spectra showing different characteristics (varying preshock velocity and density).

Clearly, the model predictions of Table 6 cover the range of line ratios found in the objects of our sample, as can be seen in Figure , and offer a suitable scenario to explain the origin of the coronal lines in AGNs. The advantage of this approach over previous ones, e.g. the Pier & Voit (1995) model, is that here the interaction between the evaporated material and the surrounding gas is taken into account. Since not all clouds have the same preshock velocity, V_s , and density, n_0 , even though they

are subjected to the same radiation field, the ionization structure among individual clouds varies. A particular line ratio is favored over the others according to the initial conditions. As an example, model 29 (M29; $V_s=200\text{ km s}^{-1}$, $n_0=200\text{ cm}^{-3}$) emits preferentially [Si VI], while model 47 (M47; $V_s=100\text{ km s}^{-1}$, $n_0=300\text{ cm}^{-3}$) favors the emission of [Fe X]. The predominance of a particular set of clouds leads to the enhancement of a given line within the CLR. As a result, there is a natural scatter in CLR ratios, as observed. Under the assumed conditions the clouds are poor emitters of intermediate and low ionization lines. These would be produced farther out in the NLR.

We have also compared the dereddened line ratios to those predicted by a pure photoionization model (see last column of Table 6), calculated by Oliva et al. (1994) assuming the “standard AGN continuum” of CLOUDY, solar abundances and $Q(\text{H})=2\times10^{52}\text{ s}^{-1}$. It can be seen that although some line ratios are in reasonable good agreement with those observed, it is not possible to reproduced the whole CLR spectrum of a single object by pure photoionization. This gives stronger support to the idea that the high ionization lines arise from a set of emitting clouds having different physical conditions. The observed spectra would result from the combination of the individual cloud spectra.

Quantitatively, the model predictions also agree with the observations. From Table 13 of Contini & Viegas (2001), temperatures of up to $6\times10^5\text{ K}$ are expected from downstream gas ionized by the shock models of Table 6. This temperature is of the same order of the value derived by Erkens, Appenzeller & Wagner (1997) for the CLR in AGNs ($\sim1.2\times10^5$) using the [Fe VII] lines as temperature indicators. They, in fact, predict higher temperatures for the plasma emitting very high ionization lines, such us [Fe X] and [Fe XI].

The absence of coronal lines in some of the objects can be explained if the photoionizing radiation from the central source that reaches the evaporated material is somewhat diminished before reaching the torus. It is also possible that orientation effects between the observer and the flow shields the emission from the CLR – i.e., most clouds are redshifted and obscured from our line of sight. This might be the case for MRK 1044 and TON S 180, which present a very weak CLR spectra. However, the hydrogen column density N_{H} of these objects, measured from X-ray observations, show little or no excess of neutral H over the Galactic value as is observed in columns 6 and 7 of Table 1). Another possibility is that coronal line emitting material in the line of sight is absent, or there is a high anisotropy in the continuum radiation that reaches the NLR. Interestingly, low to intermediate forbidden lines in the optical region for the above two sources are also very weak or absent (Comastri et al. 1998), contrary to what is seen in the remaining objects. Although the study of the reasons for the lack of coronal lines in some Seyferts is out of the scope of this paper, it is important to note that the observational evidence presented here suggests that both low and high ionization lines may have a common origin. It is certainly a question that deserves to be explored.

6. NEAR-INFRARED LOW IONIZATION LINES

Along with the forbidden high ionization lines, already discussed in the above sections, forbidden low-ionization and molecular lines are also present in the spectra. Although they may not be fully associated with the AGN, it is instructive to comment about the physical processes that can give rise to them to complement the picture already outlined for the nuclear re-

gions of the galaxies under consideration. The small width observed in low-ionization and molecular lines suggests that they are formed in the outer portions of the NLR, where, in addition to the radiation from the central source, thermal processes can also contribute to the observed emission.

6.1. A short note about H_2 molecular lines

>From our observations we note the presence of molecular H_2 lines at $1.957\mu\text{m}$ and $2.121\mu\text{m}$ in ARK 564, 1H 1934-063 and NGC 863. H_2 emission is observed in a variety of sources including infrared ultraluminous and starburst galaxies and AGN (Kawara, Nishida & Gregory 1989; Kawara & Taginuchi 1993; Goodrich, Veilleux & Hill 1994; Goldader et al. 1995; Veilleux, Sanders & Kim 1999). Several mechanisms have been proposed to excite these lines and their emission line ratios can be used to test the dominant process that accounts for their observed intensity. The H_2 ratio $2.247\mu\text{m}/2.121\mu\text{m}$ is commonly used to distinguish between thermal (0.1–0.2) and UV excitation (~ 0.55) in low density regions. X-ray heating can also play a role in the excitation of the molecular gas (Alonso-Herrero et al. 1997).

We have not detected H_2 $2.247\mu\text{m}$ above 2σ confidence in any of our spectra but the observation of $2.121\mu\text{m}$ may help us to set up an upper limit to the intensity of the former line. If UV excitation were important, H_2 $2.247\mu\text{m}$ should be observed at half the intensity of $2.121\mu\text{m}$. An inspection of our data shows that $2.247\mu\text{m}$ is below the required intensity. The upper limit to its flux is $I(\lambda 2.247)=0.2\times 10^{-15}\text{ erg cm}^{-2}\text{ s}^{-1}$ and $0.4\times 10^{-15}\text{ erg cm}^{-2}\text{ s}^{-1}$ for ARK 564 and 1H 1934-063, respectively. These values imply a $2.247\mu\text{m}/2.121\mu\text{m}$ ratio of 0.17 and 0.40, respectively. For ARK 564 that value suggests thermal excitation of the H_2 lines, while for 1H 1934-063, it is closer the value expected for UV excitation. It is also possible that X-ray heating plays an active role in the formation of molecular H_2 gas. This last possibility can be evaluated through the $[\text{Fe II}]/\text{Br}\gamma$ ratio, which predicts values up to ~ 20 while in H II regions that ratio is less than 2.5. From Table 2 we obtain ratios of 0.63 and 2.84 for ARK 564 and 1H 1934-063, respectively. Those values allow us to discard X-ray emission as the dominant mechanism to excite the molecular lines in these two objects and favor thermal processes, most probably associated with star forming regions close to the AGN, to produce the H_2 molecular emission.

6.2. The $[\text{Fe II}]/[\text{P II}]$ ratio

The $[\text{Fe II}]$ lines in the NIR are useful tracers of shocks in the NLR of AGN. This hypothesis comes from the observational fact that $[\text{Fe II}]$ is weak in H II regions and planetary nebulae (where photoionization by a central source dominates) while it is strong in shock-excited filaments of supernovae remnants (Oliva et al. 2001). The reason for the increase of $[\text{Fe II}]$ emission in the later sources is attributed to the evaporation of iron-based grains by shock fronts. It implies that the abundance of Fe^+ relative to any non-refractory species (i.e. P^+), formed in the same partially ionized region, can be used to constrain the origin of the $[\text{Fe II}]$ emission.

The above can be probed by means of the $[\text{Fe II}]$ $1.257\mu\text{m}/[\text{P II}]$ $1.188\mu\text{m}$ ratio. According to Oliva et al. (2001), it is large (≥ 20) in regions excited by fast shocks while low

(≤ 2) in normal photoionized regions. For ARK 564, the only galaxy in which the $[\text{P II}]$ $1.188\mu\text{m}$ line was detected, we found that the $[\text{Fe II}]/[\text{P II}]$ ratio is 0.82, suggesting that shocks fronts have little or no importance in the production of the $[\text{Fe II}]$ emission. Oliva et al. (2001) also points out that $[\text{Fe II}]/[\text{P II}]$ almost solely depends on the Fe/P relative abundance. According to their calculations, a solar $\text{Fe}/\text{P} \simeq 100$ abundance ratio implies in a $[\text{Fe II}]/[\text{P II}] \simeq 50$ (i.e. assuming that all iron is in gaseous phase), quite near to the value measured in supernovae remnants, where fast shocks destroy most the grains. The low ratio found in ARK 564 ($[\text{Fe II}]/[\text{P II}] = 0.82$) indicates that most of the Fe is locked up into grains. We recall that $[\text{Fe II}]$ lines are preferentially emitted in the outer portions of the NLR, contrary to the place where forbidden high ionization lines of this element are formed.

7. SUMMARY

NIR coronal lines in the $0.8\text{--}2.5\mu\text{m}$ interval are studied, for the first time, in a sample of Seyfert 1 galaxies. We have found that [S VIII], [S IX], [Fe XIII], [Si VI] and [Si X] are present in most of the objects. These lines are significantly broader than low-ionization lines such as [S III], [Ca I] and [Fe II]. In addition, blueshifts of up to 550 km s^{-1} , relative to the systemic velocity of the galaxies, are measured for [Fe XIII]. The amount of blueshift is strongly correlated with FWHM and varies among the species with similar IP. These results hold when NIR data are combined with existing optical spectroscopy. Moreover, the FWHM of the broadest coronal lines is larger than that of O I $\lambda 1.128\mu\text{m}$, a pure BLR feature, but lower than broad $\text{Pa}\beta$.

The above findings give strong observational support to the picture in which coronal lines are emitted in the intermediate region between the NLR and BLR. The blueshifts and assymetries of the highest ionization lines suggest that they are formed from outflow gas, most probably associated with material evaporated from the torus. The combined effect of shocks between that material and the ambient gas and the intense radiation field from the central source would produce the observed coronal line emission. Models that take into account these two mechanisms successfully reproduce the observed values of line ratios between coronal optical and NIR lines.

Outward from the CLR, where most low- to intermediate-ionization lines are being emitted, thermal processes associated with starburst activity may give rise to the observed molecular H_2 emission, as is indicated by the value of the H_2 ratio $2.247\mu\text{m}/2.121\mu\text{m}$. Our data also report the first detection of [P II] $1.188\mu\text{m}$ and [Ni II] $1.191\mu\text{m}$ in a Seyfert 1 object. The ratio between $[\text{Fe II}]$ $1.257\mu\text{m}$ and [P II] sets important constraints on the dominant excitation mechanism for the low-ionization gas. The low value found for $[\text{Fe II}]/[\text{P II}]$ (0.82) indicates that most iron is locked up in grains, being negligible the excitation via shocks.

This research has been supported by the Fundação de Amparo a Pesquisa do Estado de São Paulo (FAPESP) to ARA, PRONEX grant 662175/1996-4 to SMV and ARA and PRONEX grant 7697100300 to MGP and ARA. The authors are grateful to an anonymous referee for comments and suggestions that helped to improve this article.

REFERENCES

Alonso-Herrero, A., Rieke, M. J., Rieke, G. H., & Ruiz, M. 1997, ApJ, 482, 747

Appenzeller, I., & Wagner, S. J. 1991, A&A, 250, 57

Comastri, A., Fiore, F., Guainazzi, M., Matt, G., Stirpe, G. M., Zamorani, G., Brandt, W. N., Leighly, K. M., Piro, L., Molendi, S., Parmar, A. N., Siemiginowska, A., & Puchnarewicz, E. M. 1998, A&A, 333, 31

Comastri, A., Stirpe, G. M., Vignali, C., Brandt, W. N., Leighly, K. M., Fiore, F., Guainazzi, M., Matt, G., Nicastro, F., Puchnarewicz, E. M., Siemiginowska, A. 2001, A&A, 365, 400

Contini, M., & Viegas, S. M. 1992, ApJ, 401, 481

Contini, M., & Viegas, S. M. 2001, ApJS, 132, 211

Contini, M., Almudena Prieto, M., & Viegas, S. M. 1998, ApJ, 505, 621

De Robertis, M. M., & Osterbrock, D. E. 1984, ApJ, 286, 171

De Robertis, M. M., & Osterbrock, D. E. 1984, ApJ, 301, 727

Dickey, J. M., & Lockman, F. J. 1990, ARA&A, 28, 215

Erkens, U., Appenzeller, I., & Wagner, S. 1997, A&A, 323, 707

Evans, I. N. 1988, ApJS, 67, 373

Ferguson, J. W., Korista, K. T., & Ferland, G. J. 1997, ApJS, 110, 287

Giannuzzo, E., Rieke, G. H., & Rieke, M. J. 1995, ApJ, 446, L5

Goldader, J. D., Joseph, R. D., Doyon, R., & Sanders, D. B. 1995, ApJ, 444, 97

Goodrich, R. W., Veilleux, S., Hill, G. 1994, ApJ, 422, 521

Grandi, S. A. 1978, ApJ, 221, 501

Grandi, S. A. 1980, ApJ, 238, 10

Kawara, K., Nishida, M., & Gregory, B. 1989, ApJ, 342, L55

Kawara, K., & Taginuchi, Y. 1993, ApJ, 410, L19

Korista, K. T., & Ferland, G. J. 1989, ApJ, 343, 678

Knop, R. A., Armus, L., Larkin, J. E., Matthews, K., Shupe, D. L., & Soifer, B. T. 1996, AJ, 112, 81

Marconi, A., Moorwood, A. F. M., Salvati, M., & Oliva, E. 1994, A&A, 291, 18

Marconi, A., van der Werf, P. P., Moorwood, A. F. M., & Oliva, E. 1996, A&A, 315, 335

Morris, S. L., & Ward, M. J. 1989, ApJ, 340, 713

Murphy, T. W., Soifer, B. T., Matthews, K., & Armus, L. 2000, AJ, 120, 1675

Oliva, E., & Moorwood, A. F. M. 1990, ApJ348, L5

Oliva, E., Salvati, M., Moorwood, A. F. M., & Marconi, A. 1994, A&A, 288, 457

Oliva, E., Marconi, A., Maiolino, R., Testi, L., Mannucci, F., Ghinassi, F., Licandro, J., Origlia, L., Baffa, C., Checcucci, A., Comoretto, G., Gavryushev, V., Gennari, S., Giani, E., Hunt, L. K., Lisi, F., Lorenzetti, D., Marcucci, G., Miglietta, L., Sozzi, M., Stefanini, P., & Vitali, F. 2001, A&A, 369, L5

Pfefferkorn, F., Boller, T., & Rafanelli, P. 2001, A&A, 368, 797

Pier, E. A., & Voit, G. M. 1995, ApJ, 450, 628

Porquet, D., Dumont, A.-M., Collin, S., & Mouchet, M. 1999, A&A, 341, 58

Rayner, J. T., Toomey, D. W., Onaka, P. M., Denault, A. J., Stahlberger, W. E., Watanabe, D. Y., Wang, S.-I. Infrared Astronomical Instrumentation, ed. A. M. Fowler Proc. SPIE, 3354, 468-479 (1998).

Rodríguez-Ardila, A., Pastoriza, M. G., & Donzelli, C. J. 2000, ApJS, 126, 63.

Rodríguez-Ardila, A., Viegas, S. M., Pastoriza, M. G., & Prato, L. 2002, ApJ, 565, 140

Rodríguez-Ardila, A., Viegas, S. M., Pastoriza, M. G., Prato, L., & Donzelli, C. J. 2002, ApJ, 572, 94

Schlegel, D. J., Finkbeiner, D. P., & Davis, M. 1998, ApJ, 500, 525

Thompson, R. I. 1995, ApJ, 445, 700

Veilleux, S. 1988, AJ, 95, 1695

Veilleux, S. 1991, ApJS, 75, 383

Veilleux, S., Sanders, D. B., & Kim, D. -C. 1999, ApJ, 522, 139

Viegas-Aldrovandi, S. M., & Contini, M. 1989, ApJ, 339, 689

Viegas, S. M., & Contini, M. 1994, ApJ, 428, 113

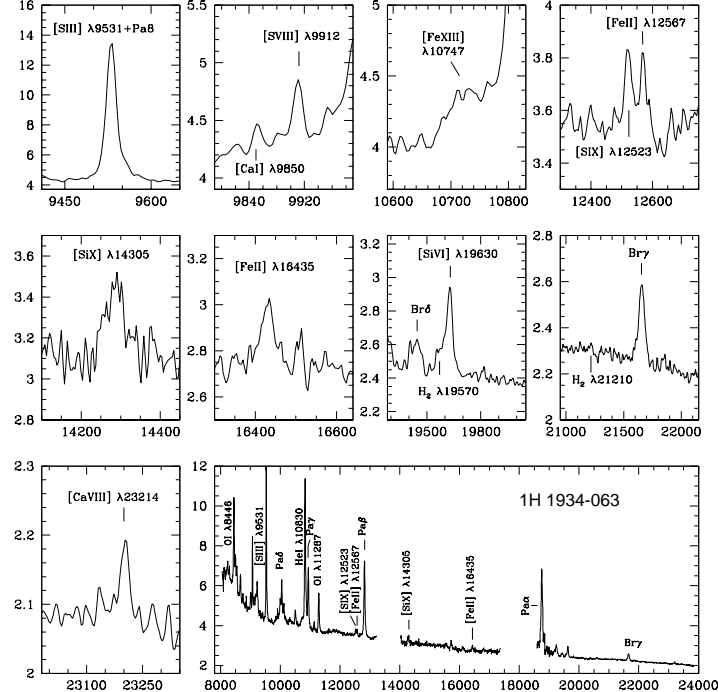


FIG. 1.—Flux calibrated spectrum of 1H 1934-063 showing, in detail, the most conspicuous NIR forbidden lines (in rest wavelength). The bottom panel shows the SpeX spectrum of the source from $0.8\mu\text{m}$ to $2.4\mu\text{m}$ with the identification of H I and other permitted and forbidden lines. Wavelengths are in Å and fluxes in units of $10^{-15} \text{ erg cm}^{-2} \text{ s}^{-1}$.

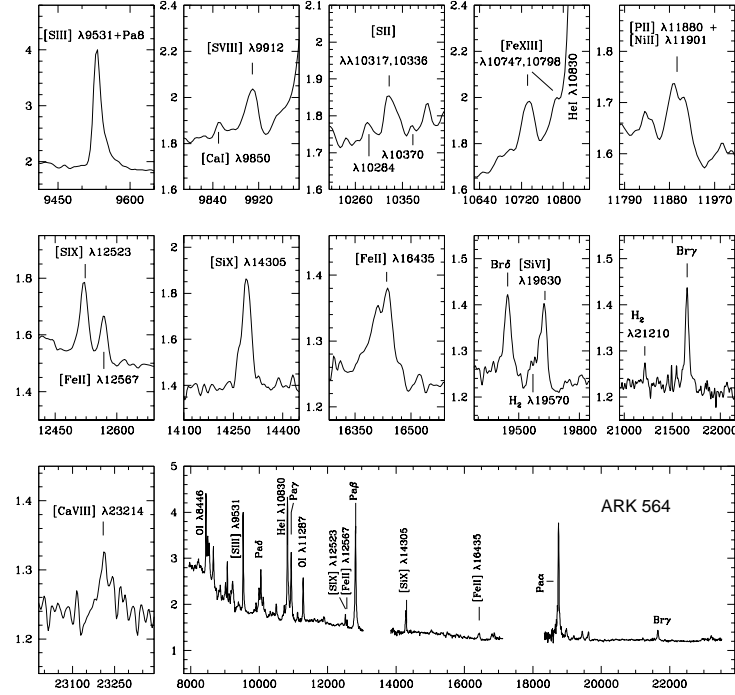


FIG. 2.— The same as Figure for ARK 564.

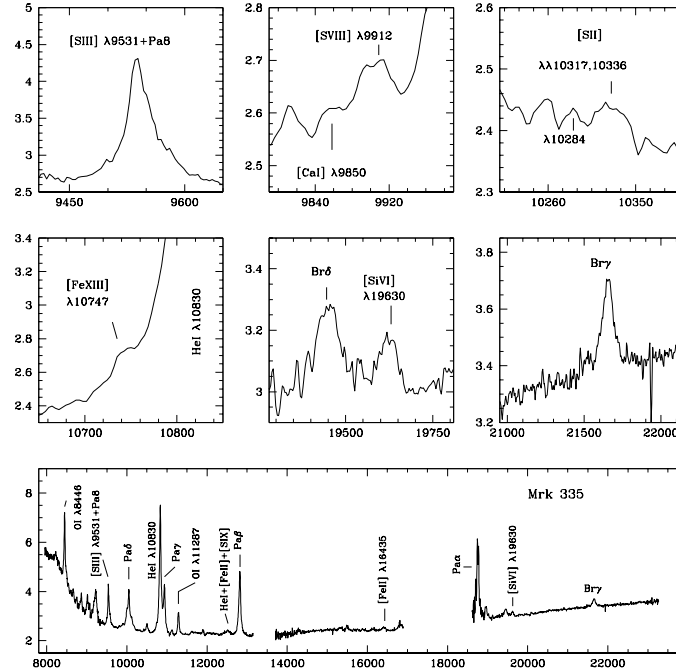


FIG. 3.— The same as Figure for MRK 335.

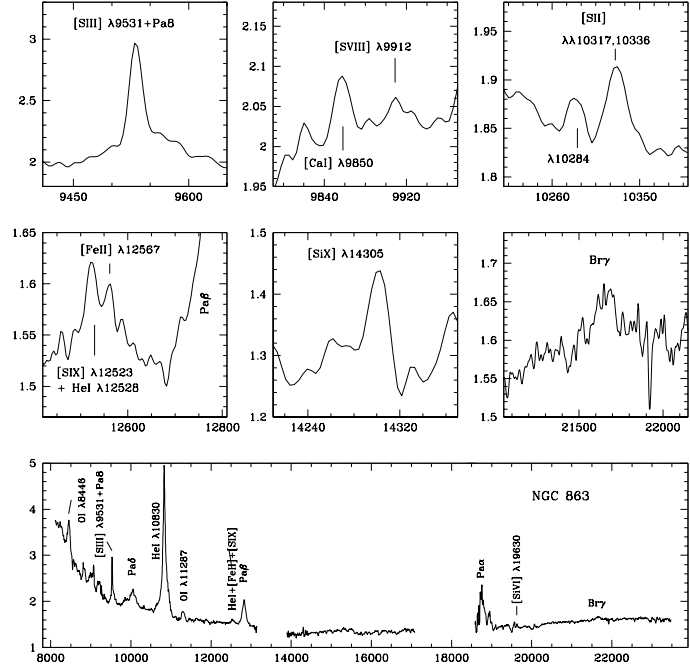


FIG. 4.— The same as Figure for NGC 863.

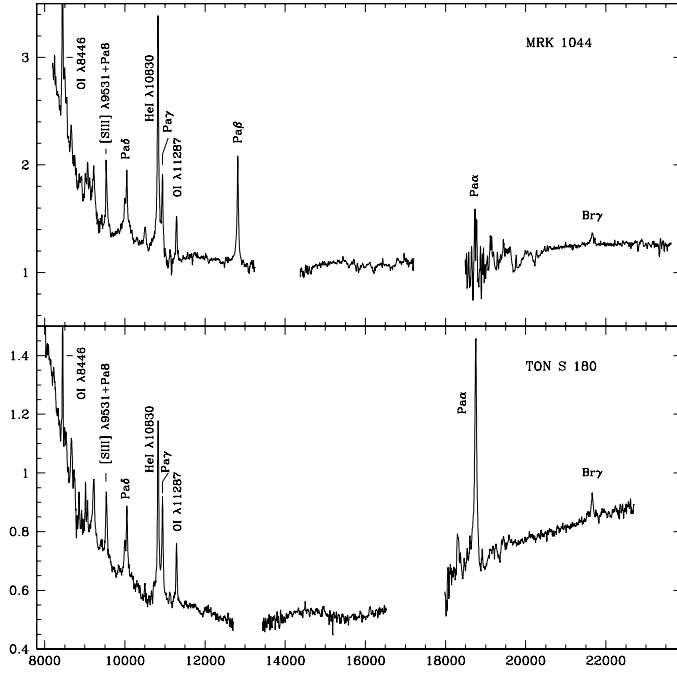


FIG. 5.— JHK spectrum of MRK 1044 (upper panel) and TON S 180 (bottom panel). Note the lack of significant coronal emission lines in these NLS1 objects.

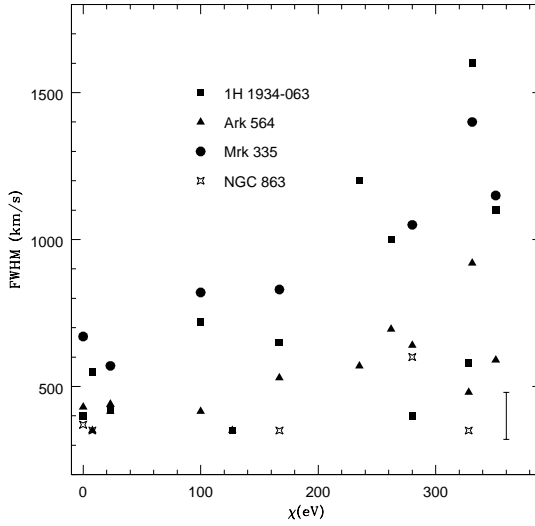


FIG. 6.— FWHM of the measured lines (already corrected for instrumental resolution) versus ionization potential. In NGC 863, except for [S VIII] 0.991 μm (IP=280 eV), the remaining forbidden emission were unresolved or detected as upper limits (see Section 4 for further details). The magnitude of the largest FWHM uncertainty is indicated by the error bar in the lower right corner.

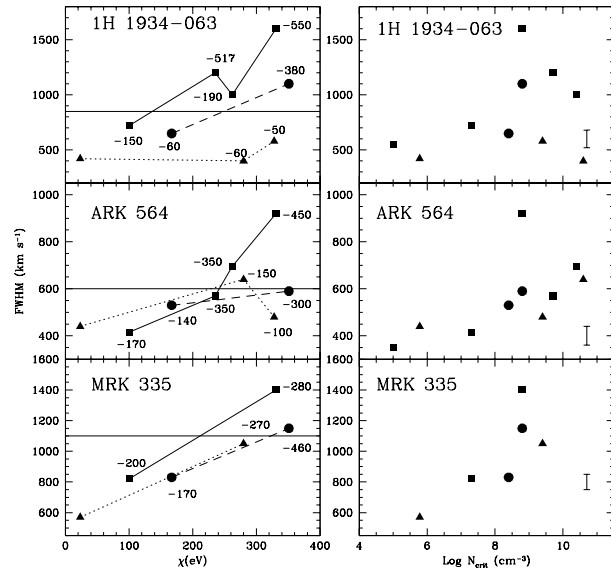


FIG. 7.— Observed FWHM versus ionization potential, χ , (left panels) and FWHM versus critical density, N_{crit} , (right panels) for 1H 1934-063 (upper panel) ARK 564 (middle panel) and MRK 335 (lower panel) by chemical specie. Squares represents iron lines; triangles, sulfur lines and circles, silicon lines. The thick line represents the FWHM of O I 1.128 μm , a pure BLR line. The magnitude of the largest FWHM uncertainty is indicated by the error bar in the right hand panels. The number beside each data point at the left panels is the shift of the line centroid regarding the systemic velocity of the galaxy. See text and Table 5 for further details.

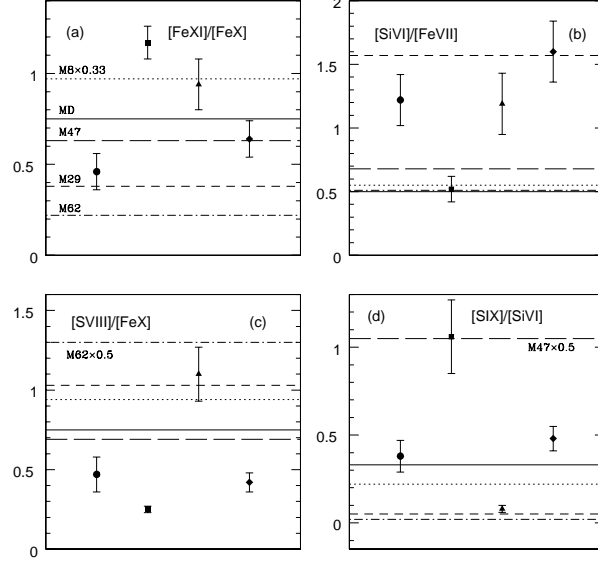


FIG. 8.— Comparison of model predictions with the observed, dereddened line ratios. 1H 1934-063 is represented by the circle, ARK 564 by the square, NGC 1068 by the triangle and Circinus by the diamond. The straight line corresponds to model MD (composite model), the dotted line to model M8 ($V_s=100 \text{ km s}^{-1}$, $n_0=100 \text{ cm}^{-3}$), the short-dashed line to model M29 ($V_s=200 \text{ km s}^{-1}$, $n_0=200 \text{ cm}^{-3}$), the long-dashed line to model M47 ($V_s=100 \text{ km s}^{-1}$, $n_0=300 \text{ cm}^{-3}$) and the dot-dashed line to model M62 ($V_s=300 \text{ km s}^{-1}$, $n_0=300 \text{ cm}^{-3}$). For visualization purposes, M8 in panel (a), M62 in panel (c) and M47 in panel (d) were multiplied by a scale factor (0.33, 0.5 and 0.5, respectively).

TABLE 1
SAMPLE CHARACTERISTICS.

Galaxy	z	M_v^a	A_v^b	Type	N_H^c	$N_{H,\text{Gal}}^d$
1H 1934-063	0.01059	-19.04	0.972	NLS1	...	18.8
Ark 564	0.02468	-20.42	0.198	NLS1	7.0 ± 0.4^1	6.4
Mrk 335	0.02578	-21.32	0.118	NLS1	3.9 ± 0.2^2	3.9 ± 0.2
Mrk 1044	0.01645	-18.84	0.113	NLS1	4.2 ± 0.4^2	3.2
TON S 180	0.06198	-22.57	0.047	NLS1	1.15 ± 0.45^3	1.48
NGC 863	0.02638	-21.27	0.124	Seyfert 1	3.17 ± 0.20^2	2.72

^aA value of $H_0 = 75 \text{ km s}^{-1} \text{ Mpc}^{-1}$ was assumed.

^bGalactic extinction (Schlegel, Finkbeiner & Davis 1998)

^cHydrogen column density, in units of 10^{20} cm^{-2} , derived from X-ray observations

^dGalactic Hydrogen column density, in units of 10^{20} cm^{-2} , derived by Dickey & Lockman (1990) from measurements of the 21-cm H I line.

References. — (1) Comastri et al. (2001); (2) Pfefferkorn, Boller & Rafanelli (2001); (3) Comastri et al. (1998).

TABLE 2
MEASURED NIR NARROW LINE FLUXES FOR THE GALAXY SAMPLE.¹

Line	1H 1934	ARK 564	MRK 335	NGC 863	MRK 1044	TONS 180
[Ca VIII] 2.321 μ m	3.94 \pm 1.10	3.12 \pm 1.00
Br γ ^b 2.165 μ m	22.4 \pm 0.14	10.50 \pm 0.6	26.70 \pm 3.1	9.34 \pm 2.60	7.80 \pm 1.5	5.30 \pm 1.00
H ₂ 2.121 μ m	1.07 ^a	1.14 \pm 0.40
[Si VI] 1.963 μ m	24.90 \pm 2.50	7.20 \pm 1.30	10.61 \pm 2.0	2.14 ^a
H ₂ 1.957 μ m	3.90 \pm 1.20	1.25 \pm 0.30	...	3.70 ^a
Br δ ^b 1.945 μ m	5.04 \pm 1.70	8.04 \pm 0.60	20.27 \pm 4.0
[Fe II] 1.644 μ m	14.33 \pm 3.50	5.10 \pm 0.80	1.85 ^a
[Si X] 1.4305 μ m	20.00 \pm 5.40	17.21 \pm 1.00	7.45 \pm 3.00	3.20 \pm 1.00
Pa β ^b 1.282 μ m	180.00 \pm 4.10	98.50 \pm 1.00	170.00 \pm 5.00	58.00 \pm 3.00	54.00 \pm 4.00	54.8 \pm 5.00 ^e
[Fe II] 1.257 μ m	7.52 \pm 2.00	3.67 \pm 0.60	...	1.00 ^a
[S IX] 1.252 μ m	9.00 \pm 2.00	7.51 \pm 0.64	12.60 \pm 2.5 ^d	1.10 \pm 0.35
[P II] 1.188 μ m	...	4.47 \pm 0.90
[Ni II] 1.191 μ m	...	1.33 \pm 0.40
[Fe XIII] 1.074 μ m	29.20 \pm 4.00	10.74 \pm 2.00	18.33 \pm 3.80	1.23 \pm 0.4
[S II] 1.030 μ m ^c	12.18 \pm 3.41	5.57 \pm 1.30	1.83 ^a	2.31 \pm 0.52	1.85 \pm 0.30	...
[S VIII] 0.991 μ m	12.30 \pm 2.80	6.54 \pm 0.40	3.76 \pm 1.00	1.00 ^a
[Ca I] 0.985 μ m	3.67 \pm 1.00	0.88 \pm 0.25	1.00 ^a	1.45 \pm 0.6	...	0.9 ^a
[S III] 0.953 μ m	165.00 \pm 3.80	31.05 \pm 1.00	22.5 \pm 2.30	15.20 \pm 0.60	20.90 \pm 0.80	2.43 ^a

¹In units of 10^{-15} erg cm $^{-2}$ s $^{-1}$.

^aUpper limit.

^bSum of broad and narrow fluxes.

^cSum of the fluxes of the [S II] lines located at 1.028 μ m and 1.032 μ m.

^dStrongly blended with He I λ 1.253.

^eFlux of Pa α .

TABLE 3
LINE RATIOS BETWEEN THE MOST IMPORTANT FORBIDDEN LINES.

Ratio	1H 1934	ARK 564	MRK 335	NGC 863	NGC 1068	Circinus ^c	NGC 4151 ^d
[Ca VIII]/H ₂ 2.121 μ m	3.68 ²	2.74 \pm 1.30	0.88 \pm 0.13	...
[Si VI]/H ₂ 1.957 μ m	6.38 \pm 2.06	5.76 \pm 1.73	...	0.57 ²	5.00 \pm 1.70 ^b	1.38 \pm 0.20	5.70 \pm 1.93
[Fe II]/[Si VI]	0.58 \pm 0.15	0.71 \pm 0.17	0.17 ¹	0.85 \pm 0.13	1.10 \pm 0.10
[Si X]/[Fe II] 1.257 μ m	2.66 \pm 1.01	4.63 \pm 0.80	...	3.2 ²
[S II]/[Fe II] 1.257 μ m	1.20 \pm 0.40	2.04 \pm 0.38	...	1.1 ²	0.65 \pm 0.10 ^a	0.34 \pm 0.05	0.17 \pm 0.04
[S II]/[S VIII]	0.99 \pm 0.35	0.65 \pm 0.15	0.49 ¹	2.31 ²	3.09 ^{a,1}
[S VIII]/[Ca I]	3.35 \pm 1.18	9.80 \pm 2.80	3.76 ²	0.69 ¹	0.77 \pm 0.12 ^a	2.00 \pm 0.30	...
[S III]/[S VIII]	13.41 \pm 3.07	4.74 \pm 0.45	5.98 \pm 1.70	15.20 ²	21.82 \pm 3.27 ^a	14.00 \pm 2.1	27.30 \pm 4.60

¹Upper limit.

²Lower limit.

References. — (a) Oliva et al. (2001); (b) Marconi et al. (1994); (c) Oliva et al. (1994); (d) Thompson (1995).

TABLE 4
OPTICAL EMISSION LINE FLUXES¹ FOR THE GALAXY SAMPLE.

Galaxy	[Fe VII] $\lambda 6087$	[Fe X] $\lambda 6374$	[Fe XI] $\lambda 7892$	E(B-V)
1H 1934	16.20 ± 2.20	23.20 ± 2.30	11.77 ± 2.50	0.10
ARK 564 ^a	13.00 ± 0.67	25.46 ± 1.51	30.40 ± 1.42	0.03
MRK 335	4.52 ± 0.57	2.14 ± 0.51	...	0.18
MRK 1044	4.36 ± 1.00	2.83^b	...	0.05
TON S 180	1.89 ± 0.60	0.00

¹In units of 10^{-15} erg cm $^{-2}$ s $^{-1}$.

^aData taken from Erkens, Appenzeller & Wagner (1997).

^bUpper limit.

TABLE 5
FWHM¹ OF CORONAL AND FORBIDDEN LOW IONIZATION LINES.

Line	χ (eV)	1H 1934		ARK 564		MRK 335		NGC 863		Log N _{crit} (cm $^{-3}$)
		FWHM	ΔV	FWHM	ΔV	FWHM	ΔV	FWHM	ΔV	
[Fe VII]	100	720	-150	420 ^c	-170 ^c	820	-200	7.3
[Fe X]	235	1200	-517	570 ^c	-350 ^c	9.7
[Fe XI]	262	1000	-190	695 ^c	-350 ^c	10.4
[S III]	23.3	420	...	440	...	570	...	420	...	5.8
[C I]	0.0	400 ^a	...	430	+60	670	+120	370	+60	4.3
[S VIII]	280	400	-60	890	-150	1050	-270	600	-90	10.6
[Fe XIII]	331	1600	-550	920	-450	1400	-280	8.8
[S IX]	328	580	-50	480	-100	350	-50	9.4
[Fe II]	7.9	550	+70	350	350	-100	5.0
[Si X]	351	1100	-380	590	-300	1150	-460	8.8
[Si VI]	167	650	-60	530	-140	830	-170	350	...	8.8
[Ca VIII]	127	350	-150	350	7.9
Pa β ^b	0.0	1800	...	1800	...	2050	...	2720
O I 1.1287 μ m	0.0	850	...	600	...	1100	...	2000

¹In km s $^{-1}$, already corrected for instrumental FWHM. The columns labeled ΔV correspond to the shift of the line relative to the systemic velocity of the galaxy. A plus sign (+) represents a redshift while a negative sign (-) a blueshift.

^aUpper limit.

^bFWHM of the broad component.

^cTaken from Erkens, Appenzeller & Wagner (1997).

TABLE 6
REDDENING CORRECTED RATIOS AMONG OPTICAL AND NIR CORONAL LINES AND MODEL PREDICTIONS.

Ratio	1H 1934	ARK 564	NGC 1068 ^a	Circinus ^b	MD ^c	M8 ^d	M29 ^d	M47 ^d	M62 ^d	PH2 ^e
[Fe X]/[Fe VII]	1.41 ± 0.23	1.95 ± 0.15	0.16 ± 0.02	1.89 ± 0.32	0.67	0.88	0.48	6.98	0.06	0.41
[Si VI]/[Fe VII]	1.22 ± 0.20	0.52 ± 0.10	1.19 ± 0.24	1.60 ± 0.24	0.50	0.55	1.57	0.68	0.51	0.81
[Fe XI]/[Fe X]	0.46 ± 0.10	1.17 ± 0.09	0.94 ± 0.14	0.64 ± 0.10	0.75	2.91	0.38	0.63	0.22	0.54
[Fe XIII]/[Fe X]	1.01 ± 0.17	0.40 ± 0.08
[S VIII]/[Fe X]	0.47 ± 0.11	0.25 ± 0.02	1.1 ± 0.17	0.42 ± 0.06	0.75	0.94	1.03	0.69	2.60	0.34
[S IX]/[Si VI]	0.38 ± 0.09	1.06 ± 0.21	0.08 ± 0.02	0.48 ± 0.07	0.33	0.22	0.05	2.1	0.02	0.06

^aTaken from Marconi et al. (1996).

^bTaken from Oliva et al. (1994).

^cModel label MD from Contini, Prieto & Viegas (1998).

^dM8, M29, M47 and M62 stand for models numbered 8, 29, 47 and 62 in Contini & Viegas (2001).

^eLine ratios predicted by a pure photoionization model assuming the standard AGN continuum, taken from Oliva et al. (1994).